Intrinsic bandgap of cleaved ZnO$(11\bar{2}0)$ surfaces

A. Sabitova,[1,a)] Ph. Ebert,[1,b)] A. Lenz,[2] S. Schaafhausen,[1] L. Ivanova,[2] M. Dähne,[2] A. Hoffmann,[2] R. E. Dunin-Borkowski,[1] A. Förster,[3] B. Grandidier,[4] and H. Eisele[2,c)]
[1]*Peter Grünberg Institut, Forschungszentrum Jülich GmbH, 52425 Jülich, Germany*
[2]*Institut für Festkörperphysik, Technische Universität Berlin, Hardenbergstr. 36, 10623 Berlin, Germany*
[3]*Institut für Nano- und Biotechnologien (INB), FH Aachen, Heinrich-Mußmann-Str. 1, 52428 Jülich, Germany*
[4]*Institut d'Electronique, de Microélectronique et de Nanotechnologie, IEMN (CNRS, UMR 8520), Département ISEN, 41 bd Vauban, 59046 Lille Cedex, France*

(Received 19 November 2012; accepted 31 December 2012; published online 18 January 2013)

The existence of intrinsic surface states, the position of the Fermi level, and the size of the surface bandgap of the non-polar ZnO$(11\bar{2}0)$ cleavage surfaces were investigated by scanning tunneling microscopy and spectroscopy. The comparison of spectroscopic measurements performed on atomically flat and stepped surfaces reveals the absence of intrinsic surface states within the fundamental bulk bandgap, but shows the occurrence of step-induced gap states. These states lead to a pinning of the Fermi level at the surface within the bandgap and generate a significant defect-related tunnel current, narrowing the measured apparent bandgap. © *2013 American Institute of Physics*. [http://dx.doi.org/10.1063/1.4776674]

Zinc oxide (ZnO) attracted wide attention due to its manifold potential applications.[1] However, the growth and incorporation of impurities, dopant atoms, and defects are still a major challenge[2] and limit the fabrication of reproducible high quality devices. Among other effects, the dopant and defect incorporation during growth[3] are affected by the structural and electronic properties of the growth surface. In particular, the Fermi-level position and the presence of intrinsic surface states within the fundamental bandgap critically influence the incorporation of dopant atoms.

Thus far, the polar crystal directions of wurtzite ZnO are the preferred growth directions. However, along these directions, electric fields and spontaneous polarization are detrimental to optoelectronic applications. This can be avoided using non-polar growth directions, where out-of-plane electric fields and spontaneous polarization effects are absent. The physical properties of non-polar ZnO surfaces were investigated theoretically[4–7] and experimentally by low energy electron diffraction (LEED),[8–10] scanning tunneling microscopy (STM) and/or spectroscopy (STS),[11–13] and other surface sensitive techniques.[14–17] It is generally accepted that non-polar $(11\bar{2}0)$ and $(10\bar{1}0)$ ZnO surfaces exhibit a 1×1 surface unit cell, where the surface oxygen atom relaxes slightly outward, while the surface zinc atom becomes more sp^2 hybridized. This relaxation is combined with a charge transfer from Zn to O, but the resulting electronic properties are strongly debated: Some calculations predict that the intrinsic surface states are outside of the fundamental bulk bandgap,[4,5] while a newer calculation suggests intrinsic surface states within the fundamental bandgap, at least for the $(10\bar{1}0)$ surface.[7] In STS spectra, the *apparent surface bandgaps* range from ~2.0 eV (Ref. 11) down to 1.0 eV.[12] Thus far, no STS measurement exhibits a surface bandgap consistent with that of the bulk (~3.5 eV), suggesting the presence of intrinsic surface states within the bandgap. Work function measurements are inconclusive too, as some suggest a flat band situation[14] and thus the absence of intrinsic surface states in the fundamental bandgap, whereas others suggest a band bending at the $(10\bar{1}0)$ surface.[16] Angular-resolved photoemission[18] and electron energy loss spectroscopy experiments[17] find no surface states within the fundamental bandgap. Over all, the electronic properties of non-polar ZnO surfaces are unclear.

Therefore, we investigated ZnO$(11\bar{2}0)$ *cleavage* surfaces by STM and STS, focusing on the determination of the surface bandgap and the energetic position of the intrinsic surface states. In contrast to previous STM/STS investigations, we cleaved the ZnO samples inside the UHV to obtain clean and stoichiometric surfaces,[19] while surfaces prepared by sputtering and thermal cleaning exhibit a high defect concentration.[11–13] Such defects may affect the electronic properties. Therefore, we compare cleavage surfaces with low and high step densities, where the steps behave as defects. The surface with low step density shows strong tip-induced band bending and no indications of intrinsic surface states in the fundamental bandgap. The highly stepped surface is pinned and exhibits a bandgap with an energetic width in the order of that in the bulk. Within this bandgap a defect-induced current, related to the step-induced electronic states, leads to an apparently reduced bandgap.

The investigated samples were cut from ZnO(0001) wafers from Cermet Inc. and Tokio Denpa with an *n*-type carrier concentration in the low $10^{17}\,cm^{-3}$ range. Ohmic contacts were prepared by sputtering a gold layer, which is intermixed with the underlying ZnO by electrical discharges followed by a second sputtered gold layer. The samples were cleaved in ultrahigh vacuum ($p \leq 1 \times 10^{-8}$ Pa). The exposed clean $(11\bar{2}0)$ surfaces were directly investigated by STM in the constant-current mode. The tunneling spectra were

[a)]Present address: Center for Energy Research, Nazarbayev University, Astana, Kazakhstan.
[b)]email: p.ebert@fz-juelich.de.
[c)]email: holger.eisele@physik.tu-berlin.de.

acquired using fixed tip-sample separations. The tip-sample separations were adjusted by the feedback loop using set voltages (V_{set}) and set currents (I_{set}).

Figure 1(a) shows a STM image of a ZnO$(11\bar{2}0)$ cleavage surface consisting of large terraces with only few single atomic monolayer (1 ML = 2.815 Å) high steps. Figure 1(b) shows the current-voltage spectrum measured on the terraces far away from the steps. It exhibits a voltage range without detectable current (detection limit ~1 pA) labeled *apparent* bandgap (E_{app}). The apparent bandgap is significantly larger than the bulk bandgap $E_{g,bulk} \approx 3.5$ eV. However, the region marked E_{app} cannot be taken directly as bandgap, since it varies with the tip-induced band bending, which drags the bands downward (upward) at negative (positive) sample voltages.[20] This shifts the onset voltages of tunneling into (out of) the conduction (valence) band to larger absolute voltage values. Hence, the voltage region without tunnel current is enlarged as compared to an ideal flat band situation. Tip-induced band bending can occur only if no Fermi level pinning by surface states exists. Thus, the wide apparent bandgap suggests the absence of intrinsic surface states within the fundamental bulk bandgap.

This conclusion is apparently in contrast to all previously published STS data of non-polar ZnO surfaces.[11,12] Previous STM/STS investigations were made on surfaces cleaned by sputter and annealing cycles.[11–13] Such surfaces exhibited high step densities. In order to elucidate the situation, we investigated a ZnO$(11\bar{2}0)$ cleavage surface, with a high density of steps, separating small $(11\bar{2}0)$ terraces with a size of 2 nm × 10 nm [Fig. 2(a)]. The steps are preferentially aligned along the [0001] direction. This step pattern is consistent with a *miscleavage* toward the neighboring $\{10\bar{1}0\}$ plane as supported by the observed macroscopic cleavage morphology.

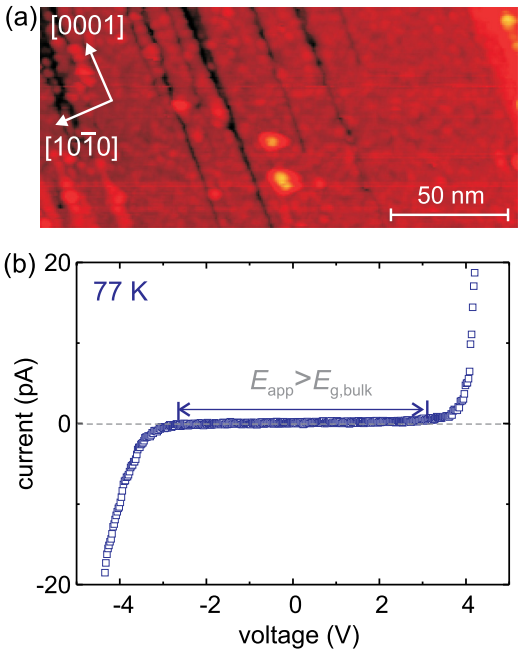

FIG. 1. (a) Constant-current empty state STM image of a ZnO$(11\bar{2}0)$ cleavage surface with few monolayer high cleavage steps measured at a voltage of $V_{set} = -5.0$ V and current of $I_{set} = 10$ pA. (b) Current-voltage (I–V) curve acquired on the terrace far away from the steps. E_{app} indicates the voltage range without detectable tunnel current, called *apparent* bandgap.

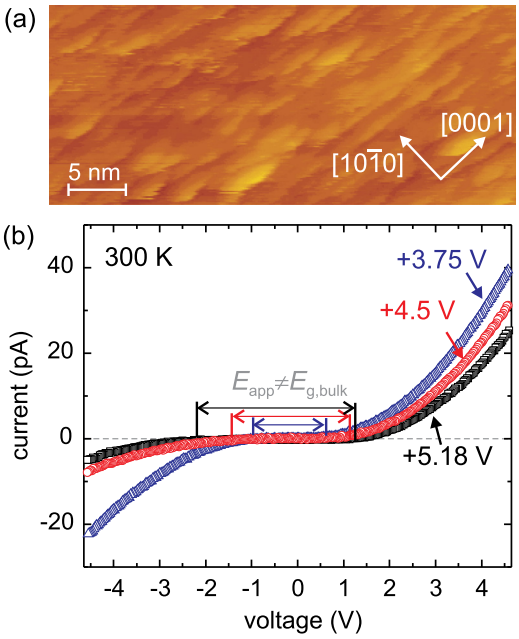

FIG. 2. (a) Constant-current empty state STM image of a stepped ZnO$(11\bar{2}0)$ cleavage surface measured at a voltage of $V_{set} = +3.6$ V and current of $I_{set} = 30$ pA. (b) Current-voltage curves (shown as symbols) acquired at the stepped ZnO$(11\bar{2}0)$ cleavage surface with different tip-sample separations, adjusted using different V_{set} as labeled. E_{app} indicates the voltage range without detectable tunnel current.

On such highly stepped cleavage surfaces, current-voltage spectra were measured with different tip-sample separations. Figure 2(b) shows the spatially averaged current-voltage curves representing the average electronic structure of the stepped surface. Due to the very small size of the terraces, it is not possible to distinguish spectra near step edges and in the center of a terrace separately as the extension of electronic step states is larger than the size of the terraces. Independent of the actual tip-sample separation, all three I–V curves exhibit again a voltage range without detectable current around 0 V (labeled E_{app}). E_{app} varies with the tip-sample separation. This effect arises from the decrease of the transmission coefficient for electron tunneling with tip-sample separation, leading to an broader voltage range without detectable tunnel current.[21] However, now the apparent bandgaps are smaller than or equal to the bulk bandgap.

In order to extract the surface bandgap, i.e., identify the band edges, we turn to the logarithmic display of the absolute current and the normalized differential conductivity $(dI/dV)/(\overline{I/V})$ as a function of the sample voltage [symbols in Figs. 3(a) and 3(b), respectively] for three tip-sample separations. First, we concentrate on the spectrum measured with the largest set voltage (+5.18 V; corresponding to the largest tip-sample separation) [black squares in Fig. 3(a)].

The logarithmically displayed current curve exhibits one clear onset of the tunnel current at positive voltages. This tunnel current is dominated by electrons tunneling into the empty conduction band states of the surface (I_C). The solid black line at positive voltages in Fig. 3(a) indicates that the onset voltage of the conduction band current is close to +1.0 V. This line represents the calculated tunnel current into the conduction band states I_C calculated following Ref.

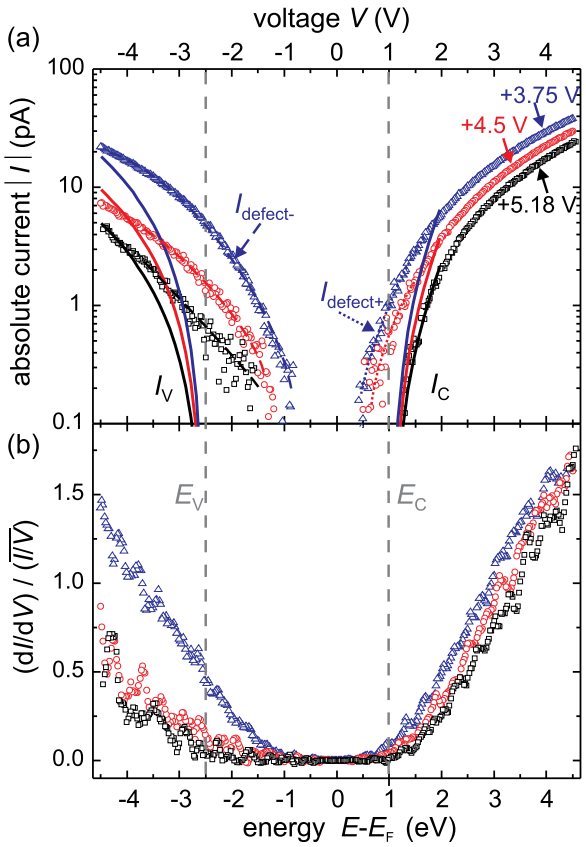

FIG. 3. (a) Absolute current-voltage spectra measured at different tip-sample separations (shown as symbols) plotted in a logarithmic display. The solid lines represent fits of the calculated tunnel current assuming only tunneling into the conduction band states or out of the valence band states. The dashed and dotted lines indicate the total current due to additional defect-related tunnel current contributions at negative ($I_{\text{defect}-}$) and positive ($I_{\text{defect}+}$) voltages, respectively. I_V and I_C denote the tunnel currents out of the valence and into the conduction band states, respectively. (b) Normalized differential conductivity $(dI/dV)/(\overline{I/V})$, shown as symbols, derived from the current-voltage spectra in (a). E_V and E_C mark the energetic positions of the valence and conduction band edges, respectively.

20 and assuming a pinning of the Fermi energy at the surface due to the presence of the surface steps.[22] The pinning has been modeled by a defect state 1 eV below the conduction band minimum with a concentration of $1 \times 10^{20}\,\text{cm}^{-3}$, being equivalent to a surface defect concentration of $\sim 2 \times 10^{12}\,\text{cm}^{-2}$. We used the ZnO bulk effective mass of the conduction band m_{cb} of 0.28 m_0, with m_0 as free electron mass. The calculated current is fitted to the experimental data by adjusting only the tip-sample separation ($z = 1.09$ nm). This value is reasonable for standard tunneling conditions, although experimentally the exact tip-sample distance is inherently not known accurately in STM.

In contrast, at negative voltages, two different tunnel current contributions are observed. Again, the solid black line at negative voltages illustrates the calculated tunnel current due to electrons tunneling out of the valence band (I_V). This calculated current is fitted to the experimental data by adjusting again the tip-sample separation ($z = 0.93$ nm). We used the bulk effective mass of the valence band m_{vb} of 0.59 m_0. It is possible to distinguish an additional tunnel current (dashed black line at voltages between $V = -2.5$ V and $V = -1.0$ V, labeled $I_{\text{defect}-}$). At voltages $V < -2.5$ V, the total current comprises both valence band and defect-related currents, i.e., $I_V + I_{\text{defect}-}$. The current $I_{\text{defect}-}$ contributes significantly at voltages representing energies within the bandgap of the ZnO, i.e., between the onset voltages of I_V and I_C. With decreasing tip-sample separation, the tunnel current contribution $I_{\text{defect}-}$ gains intensity compared with the tunnel current out of the valence band I_V (see the increasing deviation of the experimental data from the calculated current, solid red and blue lines at negative voltages). The solid red and blue lines were calculated with identical parameters as the solid black lines, but a tip-sample separation reduced by 0.03 nm and 0.06 nm, respectively. At the closest tip-sample separation, only the defect-related current contribution $I_{\text{defect}-}$ is discernable. Similarly, with decreasing tip-sample separation, an additional current contribution, labeled $I_{\text{defect}+}$, appears between 0 V and +1.0 V. Both effects shift the *apparent* onset voltages to smaller absolute values, reducing the apparent bandgap. The normalized differential conductivity $(dI/dV)/(\overline{I/V})$ curves in Fig. 3(b) exhibit analogous features as described above for the tunnel current in Fig. 3(a). However, the defect induced tunnel currents within the bandgap lead only to weak signals in the normalized differential conductivity $(dI/dV)/(\overline{I/V})$, in particular, for the larger tip-sample separations.

At this stage, we focus on the physical origins of the different contributions to the tunnel current. Figure 4 shows schematics of different band alignments of the metallic tip-ZnO surface tunnel-contact system. In general, a tunnel current only occurs if filled (empty) states at the sample surface face empty (filled) states at the tip. Due to the high step density, the Fermi energy is pinned at the surface and the tip-induced band bending is negligible. Hence, at positive sample voltages, a tunnel current occurs, if the Fermi level of the tip $E_{F,tip}$ is above the conduction band edge of the surface (I_C) [Fig. 4(b)]. Thus, the onset voltage at +1.0 V corresponds to the energetic position of the conduction band edge at the surface E_C. This indicates a Fermi level pinning of 1.0 eV below E_C. Furthermore, if $E_{F,tip}$ is below the valence band edge E_V, filled valence band states face empty tip states and electrons tunnel, yielding the I_V contribution [Fig. 4(a)]. This effect leads to the onset of the tunnel current close to a voltage of −2.5 V [Fig. 3(a)], corresponding to the valence band edge E_V at the ZnO$(11\bar{2}0)$ surface. If no states are present within the bandgap, no tunnel current should occur in a voltage range corresponding to the size of the bandgap (here −2.5 to +1 V). However, if (i) electrons accumulate at the ZnO surface due to a tip-induced band bending [Fig. 4(c)] or (ii) defects are present at the surface with extrinsic electronic states within the bandgap [Fig. 4(d)], filled (empty) semiconductor states can face empty (filled) tip states and hence a tunnel current can appear at voltages corresponding to energies within the bandgap.[20,21,23]

An electron accumulation at the sample surface, due to tip-induced band bending, requires the Fermi level to be energetically located above E_C. However, here E_F is pinned 1 eV below E_C. Thus, no charge carrier accumulation zone in the conduction band can exist. Hence, the effect of surface defects, such as steps, has to be considered. In general, steps on non-polar compound semiconductor surfaces exhibit localized charges, due to electronic states in the bandgap.[24] In analogy, steps on the ZnO cleavage surfaces are expected

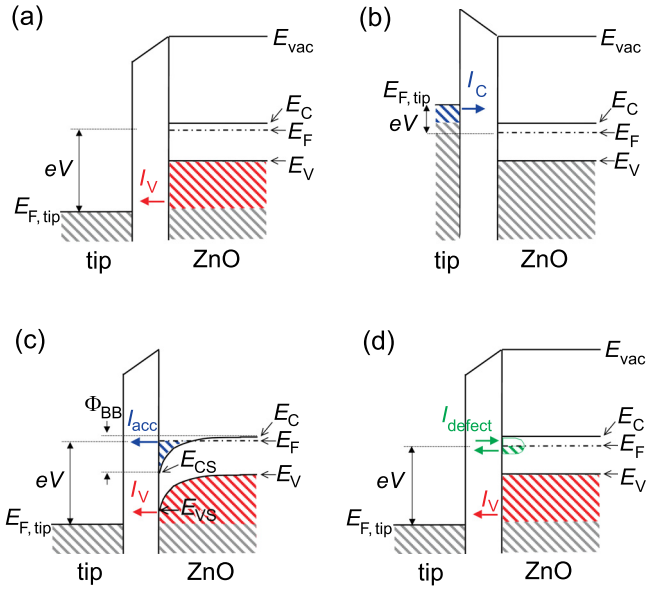

FIG. 4. Schematic of energetic band alignments of the metallic tip/vacuum barrier/n-type ZnO junction system with indicated tunnel current contributions: (a) Negative voltage V applied to the sample relative to the metallic tip. A flat band case is shown. (b) Positive voltage applied to the sample in flat band condition. I_V and I_C are the tunnel current contributions due to electrons tunneling out of the valence band or into the conduction band, respectively. (c) Effect of the tip-induced band bending (Φ_{BB}) at a negative voltage. An electron accumulation occurs at the conduction band. These electrons can lead to the accumulation tunnel current I_{acc}. (d) A surface, where a half filled band of defect states in the bandgap pins the Fermi energy. Electrons can tunnel into or out of these defect states, giving rise to a defect-related tunnel current I_{defect}. E_C, E_V, E_{CS}, E_{VS}, E_{vac} $E_{F,tip}$, and E_F correspond to the energetic positions of the conduction band edge, valence band edge, surface conduction band edge, surface valence band edge, vacuum energy, Fermi level of the tip and that of the sample, respectively.

to introduce extrinsic defect states in the bandgap. This is corroborated by the observed Fermi level pinning attributed to the high step concentration visible in Fig. 2(a). Electrons in these gap states can tunnel already at low negative voltages into empty tip states. Similarly, electrons can tunnel from the tip into the empty parts of the defect bands at low positive voltages. As a result, the tunneling spectra exhibit additional current contributions, within the voltage interval corresponding to the fundamental bandgap.[25]

Similar defect-induced currents were previously observed on GaN$(10\bar{1}0)$ and on InN$(11\bar{2}0)$ cleavage surfaces.[21,23] In these cases, the defect states could only be observed at negative voltages. This was attributed to the fact that at positive voltages, the electrons tunneling into the defect-induced gap states simply fill them and cannot be removed from there due to the lack of free holes (minority carriers) in *n*-type materials. Here, the step concentration is significantly higher as compared with cleaved GaN surfaces shown in Ref. 23. The higher step concentration leads to percolated defect bands over the whole surface, improving the carrier dynamics of electrons (or holes) injected into the defect states. Thus, also at positive voltages defect-related tunnel current contributions occur.

The above results point out the importance of defects, such as steps, on the apparent shrinking of the measured bandgap by STS. All non-polar ZnO surfaces investigated thus far by STM/STS were prepared by ion sputtering and annealing cycles and exhibited high step concentrations.[11–13] In analogy to our measurements, the defect-induced states in the bandgap not only pin the Fermi energy, but also give rise to defect-state induced tunnel currents in the bandgap. This tunnel current of *extrinsic* origin leads to apparently reduced surface bandgaps, even if no *intrinsic* surface states are located within the fundamental bandgap. Hence, non-polar ZnO$(11\bar{2}0)$ cleavage surfaces do not have intrinsic surface states within the bandgap.

[1]A. Ohtomo and M. Kawasaki, IEICE Trans. Electron. **E83-C**, 1614 (2000); K. Nomura, H. Ohta, K. Ueda, T. Kamiya, M. Hirano, and H. Hosono, Science **300**, 1269 (2003); Q. Wan, Q. H. Li, Y. J. Chen, T. H. Wang, X. L. He, J. P. Li, and C. L. Lin, Appl. Phys. Lett. **84**, 3654 (2004); Y. Ryu, T.-S. Lee, J. A. Lubguban, H. W. White, B.-J. Kim, Y.-S. Park, and C.-J. Yoon, Appl. Phys. Lett. **88**, 241108 (2006); T. Kamiya and M. Kawasaki, MRS Bull. **33**, 1061 (2008); *Zinc Oxide*, edited by C. F. Kingshirn, B. K. Meyer, A. Waag, A. Hoffmann, and J. Guerts (Springer, Heidelberg, 2010), and references therein.
[2]D. C. Look, Mater. Sci. Eng., B **80**, 383 (2001).
[3]B. K. Meyer, H. Alves, D. M. Hofmann, W. Kriegseis, D. Forster, F. Bertram, J. Christen, A. Hoffmann, M. Straßburg, M. Dworzak, U. Haboeck, and A. V. Rodina, Phys. Status Solidi B **241**, 231 (2004); M. R. Wagner, G. Callsen, J. S. Reparaz, J.-H. Schulze, R. Kirste, M. Cobet, I. A. Ostapenko, S. Rodt, C. Nenstiel, M. Kaiser, A. Hoffmann, A. V. Rodina, M. R. Phillips, S. Lautenschläger, S. Eisermann, and B. K. Meyer, Phys. Rev. B **84**, 035313 (2011).
[4]I. Ivanov and J. Pollmann, Phys. Rev. B **24**, 7275 (1981).
[5]Y. R. Wang and C. B. Duke, Surf. Sci. **192**, 309 (1987).
[6]B. Meyer and D. Marx, Phys. Rev. B **67**, 035403 (2003).
[7]N. L. Marana, V. M. Longo, E. Longo, J. B. L. Martins, and J. R. Sambrano, J. Phys. Chem. A **112**, 8958 (2008).
[8]C. B. Duke, A. R. Lubinsky, S. C. Chang, B. W. Lee, and P. Mark, Phys. Rev. B **15**, 4865 (1977).
[9]S. C. Chang and P. Mark, Surf. Sci. **45**, 721 (1974).
[10]A. R. Lubinsky, C. B. Duke, S. C. Chang, B. W. Lee, and P. Mark, J. Vac. Sci. Technol. **13**, 189 (1976).
[11]O. Dulub, L. A. Boatner, and U. Diebold, Surf. Sci. **519**, 201 (2002); U. Diebold, L. V. Koplitz, and O. Dulub, Appl. Surf. Sci. **237**, 336 (2004).
[12]X. L. Yin, A. Birkner, K. Hänel, T. Löber, U. Köhler, and C. Wöll, Phys. Chem. Chem. Phys. **8**, 1477 (2006).
[13]T. M. Parker, N. G. Condon, R. Lindsay, F. M. Leibsle, and G. Thornton, Surf. Sci. **415**, L1046 (1998); M. Kroll, T. Kuschel, T. Löber, and U. Köhler, Surf. Sci. **603**, L49 (2009).
[14]H. Moormann, D. Kohl, and G. Heiland, Surf. Sci. **80**, 261 (1979); **100**, 302 (1980).
[15]V. E. Heinrich and P. A. Cox, *The Surface Science of Metal Oxides* (Cambridge University Press, Cambridge, 1994), pp. 9–10.
[16]K. Jacobi, G. Zwicker, and A. Gutmann, Surf. Sci. **141**, 109 (1984).
[17]R. Dorn, H. Lüth, and M. Büchel, Phys. Rev. B **16**, 4675 (1977).
[18]K. Ozawa, K. Sawada, Y. Shirotori, K. Edamoto, and M. Nakatake, Phys. Rev. B **68**, 125417 (2003); K. Ozawa, K. Sawada, Y. Shirotori, and K. Edamoto, J. Phys. Condens Matter **17**, 1271 (2005).
[19]Compound semiconductor cleavage surface was shown to be stoichiometric directly after cleavage [see, e.g., B. Siemens, C. Domke, Ph. Ebert, and K. Urban, Phys. Rev. B **56**, 12321 (1997) for wurtzite structure materials and Ph. Ebert, Surf. Sci. Rep. 33, 121 (1999) and Curr. Opin. Solid State Mater. Sci. 5, 211 (2001) for zincblende materials].
[20]R. M. Feenstra and J. A. Stroscio, J. Vac. Sci. Technol. B **5**, 923 (1987); N. D. Jäger, E. R. Weber, K. Urban, and Ph. Ebert, Phys. Rev. B **67**, 165327 (2003).
[21]Ph. Ebert, S. Schaafhausen, A. Lenz, A. Sabitova, L. Ivanova, M. Dähne, Y.-L. Hong, S. Gwo, and H. Eisele, Appl. Phys. Lett. **98**, 062103 (2011).
[22]Ph. Ebert, L. Ivanova, and H. Eisele, Phys. Rev. B **80**, 085316 (2009).
[23]L. Ivanova, S. Borisova, H. Eisele, M. Dähne, A. Laubsch, and Ph. Ebert, Appl. Phys. Lett. **93**, 192110 (2008).
[24]B. Siemens, C. Domke, Ph. Ebert, and K. Urban, Phys. Rev. B **59**, 3000 (1999); M. Heinrich, C. Domke, Ph. Ebert, and K. Urban, Phys. Rev. B **53**, 10894 (1996).
[25]S. Gaan, R. M. Feenstra, Ph. Ebert, R. E. Dunin-Borkowski, J. Walker, and E. Towe, Surf. Sci. **606**, 28 (2012).